

Time-Dependent Electron Thermal Flux Inhibition in Direct-Drive Laser Implosions

Electron thermal conduction plays an important role in inertial confinement fusion (ICF):¹ it transports the laser energy absorbed near the critical surface into the overdense region and therefore directly affects the ablation process, the laser absorption, and implosion dynamics. The flux-limited Spitzer–Härm (SH) model² has been widely used to calculate the electron thermal conduction. In this model, the flux limiter f (typical value is 0.06)³ is introduced to limit the SH electron thermal flux⁴ and is given by

$$q_e = \min(fq_{\text{FS}}, q_{\text{SH}}), \quad (1)$$

where q_e is the electron thermal flux, q_{FS} is the free-streaming thermal flux defined as $q_{\text{FS}} = n_e T_e (T_e/m_e)^{1/2}$, n_e is the electron number density, T_e is the electron temperature in energy units, m_e is the electron mass, and f is the flux limiter, respectively; q_{SH} is the SH electron thermal flux.⁴ Because the flux limiter is empirically determined from the comparison between the numerical simulations and the experimental results,⁵ it depends on the experimental conditions and the experimental uncertainties.

More-general approaches to calculating the electron thermal transport include a Monte Carlo method⁶ and solving the Fokker–Planck (FP) equation. Many authors have reported that nonlocal electron thermal conduction is important, leading to a flux inhibition in laser-produced plasmas.^{7–12} This article shows that the flux inhibition is time dependent for square pulses, which affects CH target implosions.

When the mean free path of the electrons is greater than the typical temperature and gradient scale lengths in the plasma, the transport is nonlocal. To calculate the nonlocal thermal

conduction and to study its effect on the target implosions, a FP code was developed and combined with a one-dimensional hydrodynamic code (*LILAC*¹³). In our code, the electron velocity distribution function is expanded up to the $\ell = 3$ mode by Legendre polynomials of the direction cosines of the velocity vectors.¹⁴

Zeroth order:

$$\begin{aligned} \frac{\partial f_0}{\partial t} + \frac{1}{3} \left\{ \frac{\mathbf{v}}{\eta x^2} \frac{\partial}{\partial x} (x^2 f_1) - \frac{a_x}{v^2} \frac{\partial}{\partial \mathbf{v}} (v^2 f_1) \right\} \\ - \frac{2}{15 v^2} \frac{\partial U}{\partial x} \frac{\partial}{\partial \mathbf{v}} (v^3 f_2) = C_{\text{ee}} + S_0; \end{aligned} \quad (2)$$

First order:

$$\begin{aligned} \frac{\partial f_1}{\partial t} + v \frac{\partial f_0}{\partial x} - a_x \frac{\partial f_0}{\partial \mathbf{v}} \\ + \frac{2}{5} \left\{ \frac{\mathbf{v}}{x^2} \frac{\partial}{\partial x} (x^2 f_2) - \frac{a_x}{v^3} \frac{\partial}{\partial \mathbf{v}} (v^3 f_2) \right\} \\ - \frac{\partial U}{\partial x} \cdot f_1 - \left\{ \frac{2}{5} \frac{\partial U}{\partial x} + \frac{1}{5x^2} \frac{\partial}{\partial x} (x^2 U) \right\} v^2 \frac{\partial}{\partial \mathbf{v}} \left(\frac{f_1}{v} \right) \\ = -v_{\text{ei}} f_1; \end{aligned} \quad (3)$$

Second order:

$$\begin{aligned}
 & \frac{\partial f_2}{\partial t} + \mathbf{v} \frac{\partial f_1}{\partial x} - \frac{\mathbf{v}}{3x^2} \frac{\partial}{\partial x} (x^2 f_1) - \frac{2}{3} a_x \mathbf{v} \frac{\partial}{\partial \mathbf{v}} \left(\frac{f_1}{v} \right) \\
 & + \frac{3}{7} \left\{ \mathbf{v} \frac{\partial f_3}{\partial x} - \frac{a_x}{v^4} \frac{\partial}{\partial \mathbf{v}} (v^4 f_3) \right\} + \frac{1}{7} \left\{ \frac{2}{x^2} \frac{\partial (x^2 U)}{\partial x} - 4 \frac{\partial U}{\partial x} \right\} f_2 \\
 & - \left\{ \frac{\partial U}{\partial x} - \frac{1}{3x^2} \frac{\partial (x^2 U)}{\partial x} \right\} \mathbf{v} \frac{\partial f_0}{\partial x} \\
 & - \frac{1}{21} \left\{ 8 \frac{\partial U}{\partial x} + \frac{3}{x^2} \frac{\partial (x^2 U)}{\partial x} \right\} \mathbf{v} \frac{\partial f_2}{\partial \mathbf{v}} \\
 & = -3\nu_{ei} f_2; \tag{4}
 \end{aligned}$$

Third order:

$$\frac{\partial f_3}{\partial t} + \frac{3}{5} \left\{ \mathbf{v} \frac{\partial f_2}{\partial x} - a_x v^2 \frac{\partial}{\partial \mathbf{v}} \left(\frac{f_2}{v^2} \right) \right\} = -6\nu_{ei} f_3; \tag{5}$$

where f_0, f_1, f_2 , and f_3 are the $\ell = 0$ (isotropic part), 1, 2, and 3 modes of the distribution function, respectively. For the closure of these coupled equations, we use the simplified f_3 equation without the correction terms for hydrodynamic motion and nonplanar geometry; f_3 is reset to 0 at the beginning of every time step because $f_3 \ll f_2$ but $\Delta f_3 \neq 0$.

In the above equations, C_{ee} is the electron–electron collision operator,¹⁵ which is determined from the interaction of f_0 with itself only; ν_{ei} is the electron–ion collision frequency¹² given by

$$\nu_{ei} = \phi 4\pi n_e Z^* e^4 \ln \Lambda / m_e^2 v^3,$$

which effectively includes the corrections of higher-order terms neglected in the electron–electron collision operator,

$$\phi = (Z^* + 4.2) / (Z^* + 0.24).$$

The effective charge Z^* is defined by $Z^* = \langle Z^2 \rangle / \langle Z \rangle$, where $\langle Z^2 \rangle, \langle Z \rangle$ are the square of the charge and charge averaged over the ion species, respectively; e is the electron charge; $\ln \Lambda$ is the Coulomb logarithm,¹⁶ and U is the ion velocity. The acceleration term is defined as $a_x = eE_x/m_e$, where the electric field E_x is obtained from the current-free condition $j = 4\pi e/3 \int_0^\infty d\mathbf{v} v^3 f_1 = 0$. S_0 is a source term that accounts for the change in the Maxwell distribution function

$$f_M = n_e (m_e/2\pi T_e)^{3/2} \exp(-m_e v^2/2T_e),$$

i.e., $S_0 = \delta(f_M)$, due to changes in the electron density and temperature from ionization, radiation transport, laser absorption, and PdV work calculated by the hydrodynamic code before the FP calculation. The friction term η limits the temperature change due to the thermal conduction according to the real gas heat capacity per electron c_{ve} . For a real gas, η is given by $\eta = 2c_{ve}/3$, where c_{ve} is obtained from the hydrodynamic code. After the FP calculation, the effective electron temperature, defined as $T_{\text{eff}} = 2\pi/m_e \int_0^\infty f_0 v^4 d\mathbf{v}$, is returned to the hydrodynamic code. This is equivalent to solving the electron energy equation in the hydrodynamic equations.

We simulated the implosion of a polystyrene CH shell of 900- μm diameter and 20- μm thickness filled with 15 atm of D_2 gas. The 0.35- μm -wavelength laser pulse was a 1-ns-duration square starting at $t = 200$ ps with a rise time (0 to maximum) of 200 ps and a constant power of 25 TW from 0.4 ns to 1.4 ns. The irradiation intensity on the target was 9×10^{14} W/cm². Figure 90.24(a) shows the laser profile and the calculated electron thermal flux at the critical surface,

$$q_{\text{FP}} = 2\pi m_e/3 \int_0^\infty v^5 f_1 d\mathbf{v},$$

normalized by the free-streaming thermal flux at the critical surface, q_{FS} . The ratio $q_{\text{FP}}/q_{\text{FS}}$ can be defined as the flux-inhibition factor f if q_{FP} is assumed to be q_e , the “actual” flux when $f q_{\text{FS}} \leq q_{\text{SH}}$ in Eq. (1). We observe that f increases until 400 ps and then decreases with time. This shows the time dependence of the flux-inhibition factor in an ICF implosion. This time dependence of the flux inhibition is explained by the properties of the SH model and the nonlocal nature of the transport.

For the first explanation, we consider the time dependence of the relation between q_{FS} and q_{SH} , described by the SH model. At the critical surface q_{FS} is a function of the electron

temperature only, and q_{SH} is written in terms of λ_0/L_T and the free-streaming flux as $q_{SH} = 16\sqrt{2}\pi^{-1/2}(\lambda_0/L_T)q_{FS}$, where λ_0 is the electron mean free path for 90° collision scattering⁵ given by

$$\lambda_0 = v_{th}^4 / \left[4\phi\pi n_e Z^* (e^2/m_e)^2 \ln \Lambda \right],$$

where v_{th} is the thermal velocity defined by $v_{th} = (2T_e/m_e)^{1/2}$. L_T is the temperature gradient scale length defined as $T_e / (\partial T_e / \partial x)$. Figure 90.24(b) shows λ_0/L_T and electron thermal fluxes q_{FS} , q_{SH} , and q_{FP} at the critical surface. λ_0/L_T increases during the rise time of the laser pulse when T_e increases rapidly. It then decreases as L_T increases faster than λ_0 after 400 ps, at which time the constant laser pulse starts. Also, q_{FS} increases gradually with time in Fig. 90.24(b) as the

electron temperature increases gradually. This leads to q_{SH} being almost constant after 400 ps since the increase in q_{FS} and the decrease in λ_0/L_T cancel each other in contributing to q_{SH} .

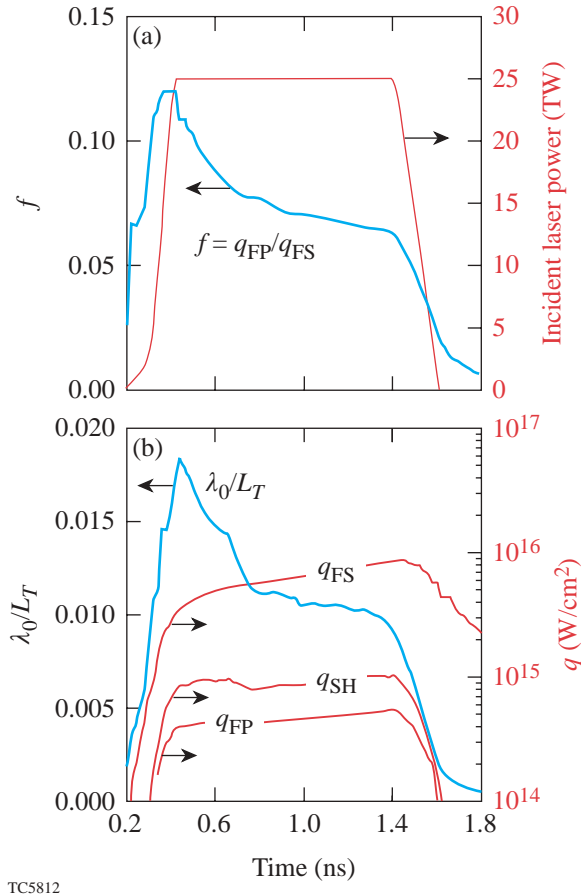
The relation between q_{SH} and q_{FP} is determined by the nonlocal transport. As seen in Fig. 90.24(b), the FP flux has a trend similar to that of the SH flux: the ratio q_{FP}/q_{SH} stays between 0.5 and 0.6 during the constant laser power. Yet, during that time, because λ_0/L_T decreases with time, we would expect the flux to be less constrained. The fact that the ratio q_{FP}/q_{SH} stays constant indicates that flux inhibition from the SH flux due to the nonlocality of the electron transport increases with time.

From the time development of the flux-inhibition factor f and the absorbed laser power I_A , the absorbed laser power-averaged flux-inhibition factor, $\langle f \rangle = \int f I_A dt / \int I_A dt$, is estimated to be 0.075 for the sharp-cutoff flux-limited SH formula of Eq. (1). We also calculated $\langle f \rangle$ with the harmonic mean flux-limited SH model, which is given by

$$q_e^{-1} = (fq_{FS})^{-1} + q_{SH}^{-1}.$$

For this model, $\langle f \rangle$ is 0.15.

The validity of our Fokker–Planck calculation is checked by comparing the calculated neutron burn history with both experimental results and results of the flux-limited SH model. The experiments were performed on the 60-beam OMEGA laser system¹⁷ with the best smoothing conditions.¹⁸ The neutron burn history was measured with the neutron temporal detector, which has a temporal accuracy of ± 50 ps.¹⁹ All the calculations were carried out with the real laser pulse and target conditions. In Fig. 90.25(a), we show three neutron rates calculated by FP and by SH with flux limiters of 0.07 and 0.06. These results are for 15-atm- D_2 gas pressure and 20- μm shell thickness irradiated by a 1-ns-duration square pulse. The results of both FP and SH with a flux limiter of 0.07 show good agreement with the experimental result. The results shown in Fig. 90.25(b) for a fuel gas pressure of 3 atm also agree well with the experimental result for a flux limiter of 0.07. The difference in amplitude between the theoretical and experimental observed rate of neutron production or the reduced burn history is believed to be caused by the shell–fuel mix during the deceleration phase due to the Rayleigh–Taylor (RT) instability.¹⁸ Results in Figs. 90.25(a) and 90.25(b) are consistent with the previous results shown in Fig. 90.24(a), where FP calculation gives $\langle f \rangle$ of 0.075. In Fig. 90.25(c), we show the



TC5812

Figure 90.24
(a) Ratio of the q_{FP} and q_{FS} measured at the critical surface; (b) ratio of λ_0 and L_T . q_{FS} and q_{SH} are calculated from the n_e and T_e obtained by FP calculation.

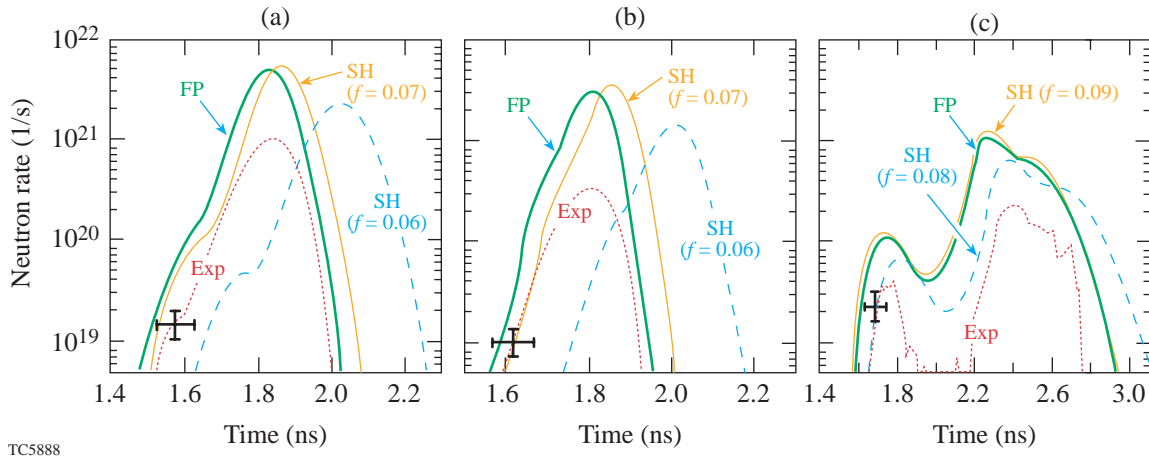


Figure 90.25

Comparison of the calculated neutron rate with results from the experiment for FP and SH with a flux limiter of 0.07 and 0.06: (a) 15 atm of D_2 fuel gas and 1-ns square pulse; (b) 3 atm of D_2 fuel and 1-ns square pulse; (c) 20 atm of DT fuel and 0.4-ns square pulse.

neutron rate for the case of a 0.4-ns square pulse (20 atm of DT in a similar target). In this case, the FP bang time agrees with that of the flux-limited SH for a flux limiter of 0.09. The experimental bang time is between SH with a flux limiter of 0.08 and FP. This indicates that a larger flux limiter is needed for short-pulse cases. In this case, $\langle f \rangle$ was found to be 0.087, which is larger than 0.075 for the 1-ns square pulse. This is consistent with the fact that a large flux-inhibition factor is needed to match the flux-limited SH flux to FP early in the pulse, as shown in Fig. 90.24(a). For all the cases shown in Figs. 90.25(a)–90.25(c), FP gives neutron temporal profiles about 50 ps ahead of these experiments. This discrepancy is within the experimental error bar. A stricter treatment of S_0 and η in Eq. (2) might reduce this discrepancy.

Next, we show the effects of the time dependence of the flux-inhibition factor on the absorption and the stability of the shell during the implosion. Due to the larger flux-inhibition factor early in the pulse, FP gives a larger thermal flux than SH with a flux limiter of 0.07, as shown in Fig. 90.24(a), resulting in a larger electron-density scale length, $L_n = n_e / (\partial n_e / \partial x)$, at the critical surface as seen in Fig. 90.26, where we also show that FP and SH with $f = 0.07$ give almost the same electron temperature T_e at the critical surface. The larger density scale length of FP at the critical surface early in the pulse gives rise to a larger absorption fraction by inverse bremsstrahlung than in the SH case as shown in Fig. 90.27, where we plot the temporal evolution of the laser absorption calculated by FP and by SH with flux limiters of 0.07 and 0.06. The laser absorption for FP is larger early in the pulse, while later in the pulse, FP

gives a lower laser absorption than SH with a flux limiter f of 0.07. The total absorption fraction is 0.83 for FP and 0.76 and 0.68 for SH with f of 0.07 and 0.06, respectively. FP gives a larger laser absorption fraction than that of the SH with 0.07 and 0.06 by about 7% and 15%, respectively.

The effect of the FP transport on the growth of the RT instability during the acceleration phase was investigated using the Betti–Goncharov formula.²⁰ In the acceleration

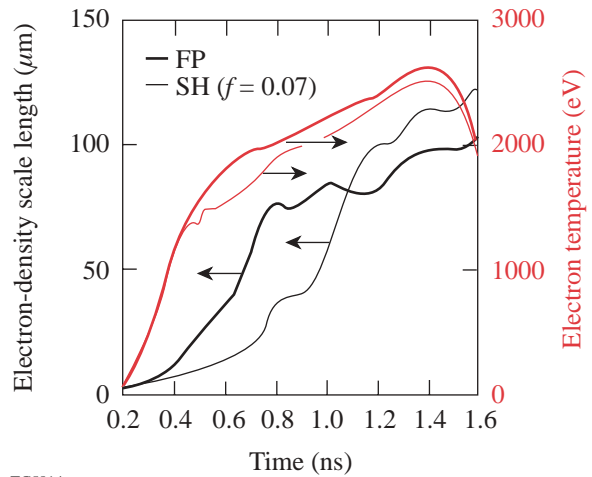


Figure 90.26

L_n and T_e for FP and SH with a flux limiter of 0.07, measured at the critical surface.

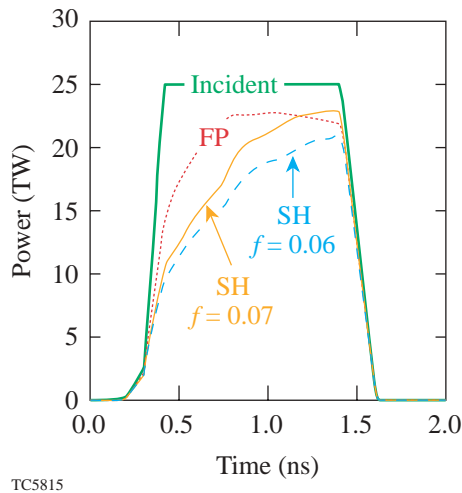


Figure 90.27

The absorbed laser power for FP and SH with flux-limiter values of 0.07 and 0.06. For reference, the incident power is also shown.

phase, the averaged ablation density $\langle \rho_a \rangle$ and the averaged mass ablation rate $\langle \dot{m} \rangle$ are 3.3 g/cm^3 and $1.35 \times 10^6 \text{ g/cm}^2 \text{ s}$ for FP and 3.9 g/cm^3 and $1.53 \times 10^6 \text{ g/cm}^2 \text{ s}$ for SH with a flux limiter of 0.07, respectively. Here, FP gives $\langle \rho_a \rangle$ and $\langle \dot{m} \rangle$ about 15% lower than that for SH. The averaged minimum density-gradient scale length $\langle L_m \rangle$ is $1.47 \text{ } \mu\text{m}$ for FP and $1.06 \text{ } \mu\text{m}$ for SH. This larger $\langle L_m \rangle$ in FP leads to stabilization of the growth of the RT instability of short-wavelength perturbations during the acceleration phase. The obtained α and β in the Betti–Goncharov formula²⁰ are 0.90 and 1.5, which are almost the same for both FP and SH.

Conclusion

Flux inhibition for square-pulse CH implosions has been shown to be time dependent. The thermal flux at the critical surface early in the pulse in the FP simulation is larger than in the flux-limited SH with a flux limiter equivalent to the averaged value calculated from the FP calculation. This was confirmed by comparing the neutron burn history from FP simulations with the experimental measurements for different fuel gas pressure and laser pulse durations. A larger flux limiter is required in simulations of implosions driven by shorter-duration pulses. The increase in the density scale length at the critical surface increases the laser absorption. The longer scale length at the ablation region also leads to a slight stabilization of the Rayleigh–Taylor growth by short-wavelength perturbations.

ACKNOWLEDGMENT

One of the authors gratefully thanks Dr. R. P. J. Town, Dr. P. W. McKenty, Dr. V. A. Goncharov, the OMEGA experiments staff of the University of Rochester's Laboratory for Laser Energetics, Prof. H. Takabe and Prof. K. Nishihara of Osaka University. This work was supported by the U.S. Department of Energy Office of Inertial Confinement Fusion under Cooperative Agreement No. DE-FC03-92SF19460, and the New York State Energy Research and Development Authority. The work was also supported by the Japan Society for Promotion of Science.

REFERENCES

1. J. Nuckolls *et al.*, *Nature* **239**, 139 (1972).
2. R. C. Malone, R. L. McCrory, and R. L. Morse, *Phys. Rev. Lett.* **34**, 721 (1975).
3. R. L. McCrory, J. M. Soures, C. P. Verdon, P. Audebert, D. Bradley, J. Delettrez, R. Hutchison, S. D. Jacobs, P. Jaanimagi, R. Keck, H. Kim, T. Kessler, J. Knauer, R. Kremens, S. Letzring, F. Marshall, P. McKenty, M. C. Richardson, A. Simon, R. Short, S. Skupsky, and B. Yaakobi, in *High Intensity Laser-Matter Interactions*, edited by E. M. Campbell and H. Baldis (SPIE, Bellingham, WA, 1988), Vol. 913, pp. 40–58.
4. L. Spitzer, Jr. and R. Härm, *Phys. Rev.* **89**, 977 (1953).
5. D. Shvarts, J. Delettrez, R. L. McCrory, and C. P. Verdon, *Phys. Rev. Lett.* **47**, 247 (1981).
6. R. J. Mason, *Phys. Rev. Lett.* **47**, 652 (1981).
7. A. R. Bell, R. G. Evans, and D. J. Nicholas, *Phys. Rev. Lett.* **46**, 243 (1981).
8. J. P. Matte and J. Virmont, *Phys. Rev. Lett.* **49**, 1936 (1982).
9. J. R. Albritton, *Phys. Rev. Lett.* **50**, 2078 (1983).
10. J. P. Matte, T. W. Johnston, J. Delettrez, and R. L. McCrory, *Phys. Rev. Lett.* **53**, 1461 (1984).
11. A. Nishiguchi *et al.*, *Phys. Fluids B* **4**, 417 (1992).
12. E. M. Epperlein, *Laser Part. Beams* **12**, 257 (1994).
13. M. C. Richardson, P. W. McKenty, F. J. Marshall, C. P. Verdon, J. M. Soures, R. L. McCrory, O. Barnouin, R. S. Craxton, J. Delettrez, R. L. Hutchison, P. A. Jaanimagi, R. Keck, T. Kessler, H. Kim, S. A. Letzring, D. M. Roback, W. Seka, S. Skupsky, B. Yaakobi, S. M. Lane, and S. Prussin, in *Laser Interaction and Related Plasma Phenomena*, edited by H. Hora and G. H. Miley (Plenum Publishing, New York, 1986), Vol. 7, pp. 421–448.
14. I. P. Shkarofsky, T. W. Johnston, and M. P. Bachynski, *The Kinetics of The Plasmas* (Addison-Wesley, Reading, MA, 1966).
15. E. M. Epperlein, *J. Comput. Phys.* **112**, 291 (1994).
16. S. Skupsky, *Phys. Rev. A* **36**, 5701 (1987).

17. T. R. Boehly, D. L. Brown, R. S. Craxton, R. L. Keck, J. P. Knauer, J. H. Kelly, T. J. Kessler, S. A. Kumpan, S. J. Loucks, S. A. Letzring, F. J. Marshall, R. L. McCrory, S. F. B. Morse, W. Seka, J. M. Soures, and C. P. Verdon, *Opt. Commun.* **133**, 495 (1997).
18. D. D. Meyerhofer, J. A. Delettrez, R. Epstein, V. Yu. Glebov, V. N. Goncharov, R. L. Keck, R. L. McCrory, P. W. McKenty, F. J. Marshall, P. B. Radha, S. P. Regan, S. Roberts, W. Seka, S. Skupsky, V. A. Smalyuk, C. Sorce, C. Stoeckl, J. M. Soures, R. P. J. Town, B. Yaakobi, J. D. Zuegel, J. Frenje, C. K. Li, R. D. Petrasso, D. G. Hicks, F. H. Séguin, K. Fletcher, S. Padalino, M. R. Freeman, N. Izumi, R. Lerche, T. W. Phillips, and T. C. Sangster, *Phys. Plasmas* **8**, 2251 (2001).
19. R. A. Lerche, D. W. Phillion, and G. L. Tietbohl, *Rev. Sci. Instrum.* **66**, 933 (1995).
20. R. Betti, V. N. Goncharov, R. L. McCrory, and C. P. Verdon, *Phys. Plasmas* **5**, 1446 (1998).